Original Article | Cardiovascular Imaging

eISSN 2005-8330
https://doi.org/10.3348/kjr.2022.0127
Korean J Radiol 2022;23(11):1044-1054

Korean Journal of Radiology
KJR

Improvement in Image Quality and Visibility of Coronary Arteries, Stents, and Valve Structures on CT Angiography by Deep Learning Reconstruction

Chuluunbaatar Otgonbaatar[1]*, Jae-Kyun Ryu[2]*, Jaemin Shin[3], Ji Young Woo[4], Jung Wook Seo[5], Hackjoon Shim[2, 6], Dae Hyun Hwang[3, 4]

[1]Department of Radiology, College of Medicine, Seoul National University, Seoul, Korea; [2]Medical Imaging AI Research Center, Canon Medical Systems Korea, Seoul, Korea; [3]Department of Radiology, Inje University Seoul Paik Hospital, Seoul, Korea; [4]Department of Radiology, Kangnam Sacred Heart Hospital, Hallym University College of Medicine, Seoul, Korea; [5]Department of Radiology, Inje University Ilsan Paik Hospital, Goyang, Korea; [6]ConnectAI Research Center, Yonsei University College of Medicine, Seoul, Korea

Objective: This study aimed to investigate whether a deep learning reconstruction (DLR) method improves the image quality, stent evaluation, and visibility of the valve apparatus in coronary computed tomography angiography (CCTA) when compared with filtered back projection (FBP) and hybrid iterative reconstruction (IR) methods.

Materials and Methods: CCTA images of 51 patients (mean age ± standard deviation [SD], 63.9 ± 9.8 years, 36 male) who underwent examination at a single institution were reconstructed using DLR, FBP, and hybrid IR methods and reviewed. CT attenuation, image noise, signal-to-noise ratio (SNR), contrast-to-noise ratio (CNR), and stent evaluation, including 10%–90% edge rise slope (ERS) and 10%–90% edge rise distance (ERD), were measured. Quantitative data are summarized as the mean ± SD. The subjective visual scores (1 for worst -5 for best) of the images were obtained for the following: overall image quality, image noise, and appearance of stent, vessel, and aortic and tricuspid valve apparatus (annulus, leaflets, papillary muscles, and chordae tendineae). These parameters were compared between the DLR, FBP, and hybrid IR methods.

Results: DLR provided higher Hounsfield unit (HU) values in the aorta and similar attenuation in the fat and muscle compared with FBP and hybrid IR. The image noise in HU was significantly lower in DLR (12.6 ± 2.2) than in hybrid IR (24.2 ± 3.0) and FBP (54.2 ± 9.5) ($p < 0.001$). The SNR and CNR were significantly higher in the DLR group than in the FBP and hybrid IR groups ($p < 0.001$). In the coronary stent, the mean value of ERS was significantly higher in DLR (1260.4 ± 242.5 HU/mm) than that of FBP (801.9 ± 170.7 HU/mm) and hybrid IR (641.9 ± 112.0 HU/mm). The mean value of ERD was measured as 0.8 ± 0.1 mm for DLR while it was 1.1 ± 0.2 mm for FBP and 1.1 ± 0.2 mm for hybrid IR. The subjective visual scores were higher in the DLR than in the images reconstructed with FBP and hybrid IR.

Conclusion: DLR reconstruction provided better images than FBP and hybrid IR reconstruction.

Keywords: *Deep learning reconstruction; Hybrid iterative reconstruction; Filtered-back projection; Coronary stent; Valve apparatus*

INTRODUCTION

Coronary computed tomography angiography (CCTA) is a widely accepted noninvasive diagnostic imaging technique to rule out coronary heart disease and is also suitable for noninvasive follow-up of coronary stenting. The evaluation of lumen stenosis or in-stent patency remains challenging because of the occurrence of blooming artifacts from the

Received: December 10, 2021 **Revised:** August 24, 2022 **Accepted:** August 26, 2022

*These authors contributed equally to this work.

Corresponding author: Dae Hyun Hwang, MD, PhD, Department of Radiology, Kangnam Sacred Heart Hospital, Hallym University College of Medicine, 1 Singil-ro, Yeongdeungpo-gu, Seoul 07441, Korea.
• E-mail: mddhhwang@naver.com; and
Hackjoon Shim, PhD, ConnectAI Research Center, Yonsei University College of Medicine, 50 Yonsei-ro, Seodaemun-gu, Seoul 03722, Korea.
• E-mail: hjshim@yuhs.ac

Korean Journal of Radiology
KJR

stent, which gives rise to a thicker appearance than the actual size and leads to an overestimation of in-stent stenosis or underestimation of the vessel size due to partial volume averaging and beam hardening artifacts [1]. Therefore, accurate evaluation of stent patency with the reduction of blooming artifacts from stents plays a crucial role in clinical settings.

In addition, CTA has been recognized as a standard technique for the preoperative assessment for transcatheter aortic valve replacement (TAVR), transcatheter mitral valve replacement (TMVR), and transcatheter tricuspid valve replacement (TTVR) [2,3]. Aortic annular and valve sizing should be measured accurately to prevent the risk of complications after the procedure [4,5]. Therefore, the clear delineation of valves with high temporal and spatial resolution images plays an important role in pre- and postoperative evaluations.

Various CT image reconstruction methods have been developed to reduce the radiation dose while maintaining the image quality, such as hybrid iterative reconstruction (IR) and model-based iterative reconstruction methods (MBIR). The recently proposed and employed deep learning reconstruction (DLR) algorithm was trained on the images generated by MBIR, referred to as an advanced intelligent clear IQ engine (Canon Medical Systems Corporation) [6,7]. In general, DLR algorithms were found to lower the image noise and improve the spatial resolution compared with filtered back projection (FBP) and hybrid IR [8].

Several studies have investigated the image quality of DLR applied to clinical images in various areas. To the best of our knowledge, no study has evaluated the effects of DLR on blooming artifacts and stent evaluation. In this study, we aimed to investigate whether the use of DLR improves image quality, stent evaluation, and visualization of the valve apparatus in CCTA when compared with FBP and hybrid IR.

MATERIALS AND METHODS

Patient Population

This retrospective study was approved by the Institutional Review Board of Inje University Seoul Paik Hospital (IRB No. 2021-06-007). From January 2021 to May 2021, 51 patients (mean age ± standard deviation [SD], 63.9 ± 9.8 years, range, 41–85 years) who had undergone CCTA at a single institution were reviewed. Of these patients, 70.6% (n = 36) were men, and the mean body mass index was 24.3 ± 3.1 kg/m^2 with a range of 17.3–33.2 kg/m^2. Fifteen patients underwent coronary artery stenting. Patients with a prior allergic reaction to iodinated contrast material, pregnancy, impaired renal function (glomerular filtration rate < 60 mL/min), or clinical instability were excluded.

CT Image Acquisition and Reconstruction

Prospective ECG-gated scanning was performed using a 320-MDCT volume scanner (Aquilion ONE PRISM; Canon Medical Systems Corporation). The detector collimation was 130 x 0.5 mm; the field of view was 320 mm; the gantry rotation speed was 0.28 seconds; the wide-volume scanning; and the tube voltage was 100 kVp. An automatic exposure control with a SD of 20 was used for the tube current. Images were reconstructed with a slice thickness of 0.5 mm. The scan was triggered using an automatic bolus-tracking program (^{SURE}Start, Canon Medical Systems Corporation) in the descending thoracic aorta (trigger threshold was 250 Hounsfield units [HU]). A bolus of 80 mL iohexol-370 contrast material (Bonorex 370; Central Medical Service Co., Ltd) was injected into the antecubital vein at the rate of 4.5 mL/sec via an ulrich CT motion Injector (CT motion, ulrich GmbH & Co. KG) followed by a 30 mL saline flush at a rate of 5.0 mL/s. All examinations were performed using prospective electrocardiography triggering methods covering 30%–85% of the cardiac cycle in the patients. We calculated the effective radiation dose (ED) for each patient using the following formula: ED = dose-length product (DLP) x conversion coefficient for the chest (κ = 0.014 mSv/mGy·cm) [9]. The raw data were retrieved from a CT scanner and reconstructed using the following three algorithms: FBP, hybrid IR with medium sharp kernel-FC14 (Adaptive Iterative Dose Reduction 3-D, AIDR-3D [9,10], Canon Medical Systems Corporation), and DLR with body sharp option (AiCE, Canon Medical Systems Corporation). CTA images were sent to a workstation for analysis (Vitrea, Vital).

Objective Image Analysis

An experienced radiologist performed all objective image analyses. Image noise, CT attenuation, signal-to-noise ratio (SNR), and contrast-to-noise ratio (CNR) were calculated at the same position in all three image datasets reconstructed with FBP, hybrid IR, and DLR for each patient. Image noise was determined as the SD of HU by placing a region of interest (ROI; 70 mm^2) in the subcutaneous fat. The SNR was calculated by dividing each attenuation value of the main coronary arteries (right coronary artery, left main

 https://doi.org/10.3348/kjr.2022.0127

coronary artery, left circumflex artery, and left anterior descending artery) by image noise. CNR was measured as the difference between the HU value of the coronary arteries and that of the left pectoralis major muscle, which was then divided by the image noise. The largest possible size of the ROIs at the center of the main coronary arteries was used depending on the diameter of each vessel while avoiding the inclusion of the vessel wall. To investigate the contrast increase effect of DLR, a histogram analysis was performed for the root of the aorta, subcutaneous fat, and pectoralis major muscle by placing an ROI size of 100 mm^2 for the aortic root, 15 mm^2 for the subcutaneous fat, and pectoral major muscle on seven consecutive slices (Fig. 1). Histogram analysis was performed offline using MATLAB (ver.8.2.0; Mathworks).

Coronary Artery Stent Assessment

The window settings (window level, 500 HU; width, 1500 HU) were fixed to improve stent delineation. The coronary artery stent assessment was performed by an experienced radiologist. On an axial image of each stent, the CT attenuation profile was determined along a horizontal line through the center of the stent. Then, the 10%–90% edge rise distance (ERD), 10%–90% edge rise slope (ERS), and peak CT attenuation were calculated or measured along the profile. The peak CT attenuation number is the maximum value of the CT attenuation profile. The 10%–90% ERD was defined as the distance between 10% and 90% of the peak CT attenuation value. A shorter edge distance demonstrates higher sharpness. The 10%–90% ERS was determined as ($CT_{90\%}$–$CT_{10\%}$)/ERD [11]. In addition, the diameter of the coronary stent was measured by the peak-to-peak distance of the stent strut on both sides opposite to each other (Fig. 2). To minimize the risk of stent assessment fluctuations, an experienced radiologist manipulated the imaging data. All measurements were

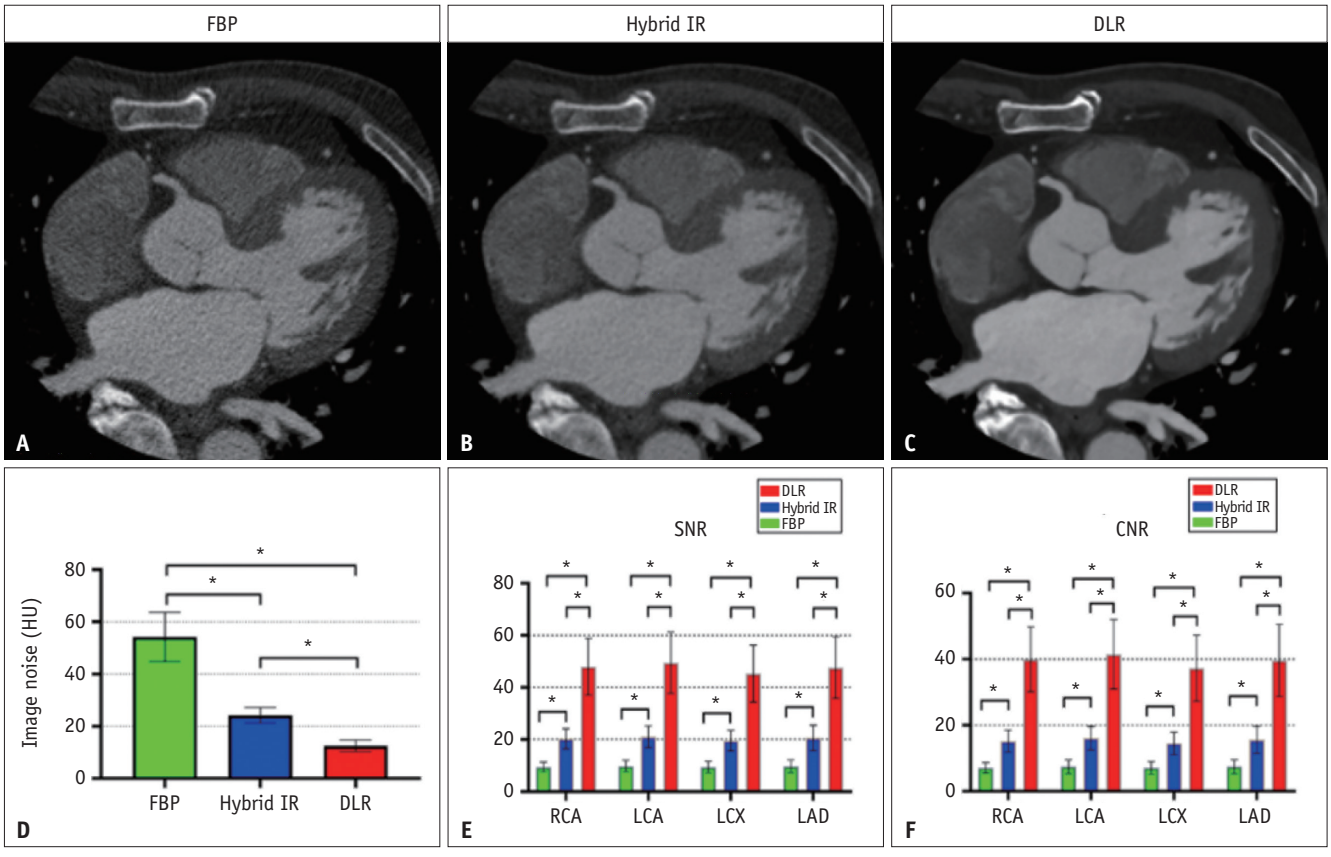

Fig. 1. The quantitative image analysis in FBP, hybrid IR, and DLR.
A-F. The coronary CT angiography (top) demonstrates improved overall image quality in DLR **(C)** compared with hybrid IR **(B)** and FBP **(A)**. In the bar graph (bottom), the image noise **(D)** is significantly reduced; higher SNR **(E)** and CNR **(F)** are found in DLR (red color) than FBP (green color) and hybrid IR (blue color). The length of the error were shown as standard deviations. *Indicates $p < 0.001$. CNR = contrast-to-noise ratio, DLR = deep learning reconstruction, FBP = filtered back projection, HU = Hounsfield unit, IR = iterative reconstruction, LAD = left anterior descending artery, LCA = left main coronary artery, LCX = left circumflex artery, RCA = right coronary artery, SNR = signal-to-noise ratio

https://doi.org/10.3348/kjr.2022.0127

Korean Journal of Radiology
KJR

performed at the same location on the proximal, middle, and distal parts of the stent on both sides. The normalized profile curves of the stent struts were compared between images reconstructed by FBP, hybrid IR, and DLR to assess the blooming artifacts arising from the metallic stent struts using ImageJ software (The National Institutes of Health), Medical Imaging Processing, Analysis, and Visualization (MIPAV) (http://mipav.cit.nih.gov/), and MATLAB.

Subjective Image Analysis

Two experienced radiologists (with 3 years and over 20 years of experience in diagnostic radiology) independently evaluated image quality. The radiologists were blinded to the image reconstruction algorithms and randomly evaluated the CTA images; the results were averaged for subjective analysis. A five-point Likert scale was used for image analysis in the following six aspects: overall image quality, image noise, and appearance of stent, vessel, and aortic and tricuspid valve apparatus (including annulus, leaflets, papillary muscles, and chordae tendineae) (Table 1) [12,13].

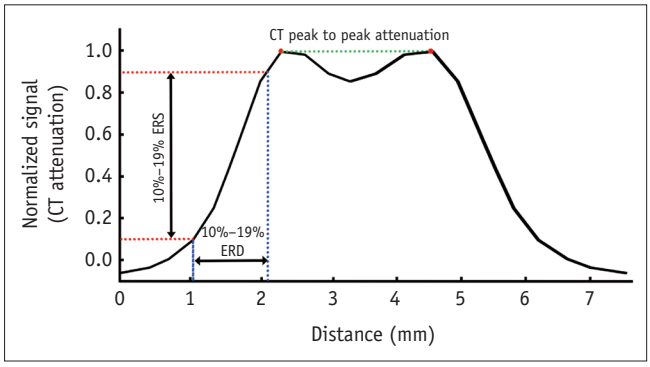

Fig. 2. Coronary artery stent analysis with 10%–90% ERD, 10%–90% ERS, and CT peak to peak attenuation. The peak CT attenuation number is recorded on the CT attenuation profile and calculated the 10%–90% ERD (blue dashed line) as the distance of 10% and 90% of the peak CT attenuation profile that corresponding to the vascular wall and lumen boundary. A shorter edge distance demonstrates a higher sharpness. The 10%–90% ERS (red dashed line) was determined as follows: $(CT_{90\%}–CT_{10\%})$/ERD. In addition, the diameter of the coronary stent was measured by the peak-to-peak CT attenuation of stent strut (green dashed line) on both sides. ERD = edge rise distance, ERS = edge rise slope

Statistical Analyses

Continuous variables are represented as mean and SD. The Kolmogorov–Smirnov test was used to evaluate normality. The image noise, CT attenuation, SNR, CNR, ERD, and ERS among the three image reconstruction methods were compared using one-way ANOVA. Tukey's test was used for post hoc pairwise multiple comparisons. The subjective analysis was compared with the Kruskal–Wallis test among different image reconstruction methods and the pairwise analysis with Wilcoxon-signed rank test. Agreement among the diameters of the coronary stents of the three reconstruction methods was assessed using the intraclass correlation coefficient (ICC). The mean differences and

Table 2. Patient Chracteristics

Total number of patients	51
Age, years	63.9 ± 9.8 (41–85)
Male sex	36 (70.6)
BMI, kg/m^2	24.3 ± 3.1 (17.3–33.2)
Medical history	
Diabetes	7 (13.7)
Hypertension	10 (19.6)
Hyperlipidemia	8 (15.7)
Family history of CVD	4 (7.8)
Smoking	
Former smokers	4 (7.8)
Ex-smokers	3 (5.9)

Data are presented as mean ± standard deviation (range). Otherwise, data are number of patients with % in parentheses. BMI = body mass index, CVD = cardiobascular disease

Table 1. Scoring for Subjective Image Analysis

Score	Overall Image Quality	Image Noise	Stent Appearance	Vessel and Lumen	Aortic and Tricuspid Valve Apparatus
5	Excellent image quality	Minimal noise	Very clear stent strut margin	Excellent delineation of vessel and lumen	Sharp defined
4	Good image quality	Average noise	Clear stent strut margin definition	Good delineation of vessel and lumen	Slightly blurred
3	Moderate image quality	Moderate noise	Moderate stent margin	Moderate delineation of vessel and lumen	Moderated blurred
2	Poor image quality	Marked noise	Poor stent margin	Poor delineation of vessel and lumen	Fairly blurred
1	Insufficient image quality and non-diagnostic	Severe noise	Impossible to evaluate stent strut	Very poor delineation of vessels and lumen	Highly blurred and non-diagnostic

https://doi.org/10.3348/kjr.2022.0127

95% limits of agreement were illustrated using the Bland-Altman plot. The interobserver agreement in the qualitative evaluation was assessed with Cohen's kappa coefficient (κ), where a κ value of less than 0.2 = poor, 0.3–0.4 = fair, 0.4–0.6 = moderate, 0.6–0.8 = substantial, and 0.8–1.0 = near-perfect agreement, respectively. All statistical analyses were performed using the SPSS statistical software ver. 25.0 (IBM Corp.). Statistical significance was set at $p < 0.05$.

RESULTS

Patient characteristics are summarized in Table 2. The mean DLP was 194.3 ± 95.1 mGy·cm, and the mean CT dose index volume was 13.2 ± 6.5 mGy. The mean ED was 2.3 ± 1.6 mSv.

Objective Image Analysis

The quantitative measurements of the image quality, including the image noise, SNR, and CNR values, are summarized in Figure 2. The image noise in HU was significantly lower in DLR (12.6 ± 2.2) by 48.1% and 76.8% than in hybrid IR (24.2 ± 3.0) and FBP (54.2 ± 9.5), respectively, with statistical significance (FBP vs. hybrid IR, and FBP vs. DLR, and hybrid IR vs. DLR, respectively; $p <$

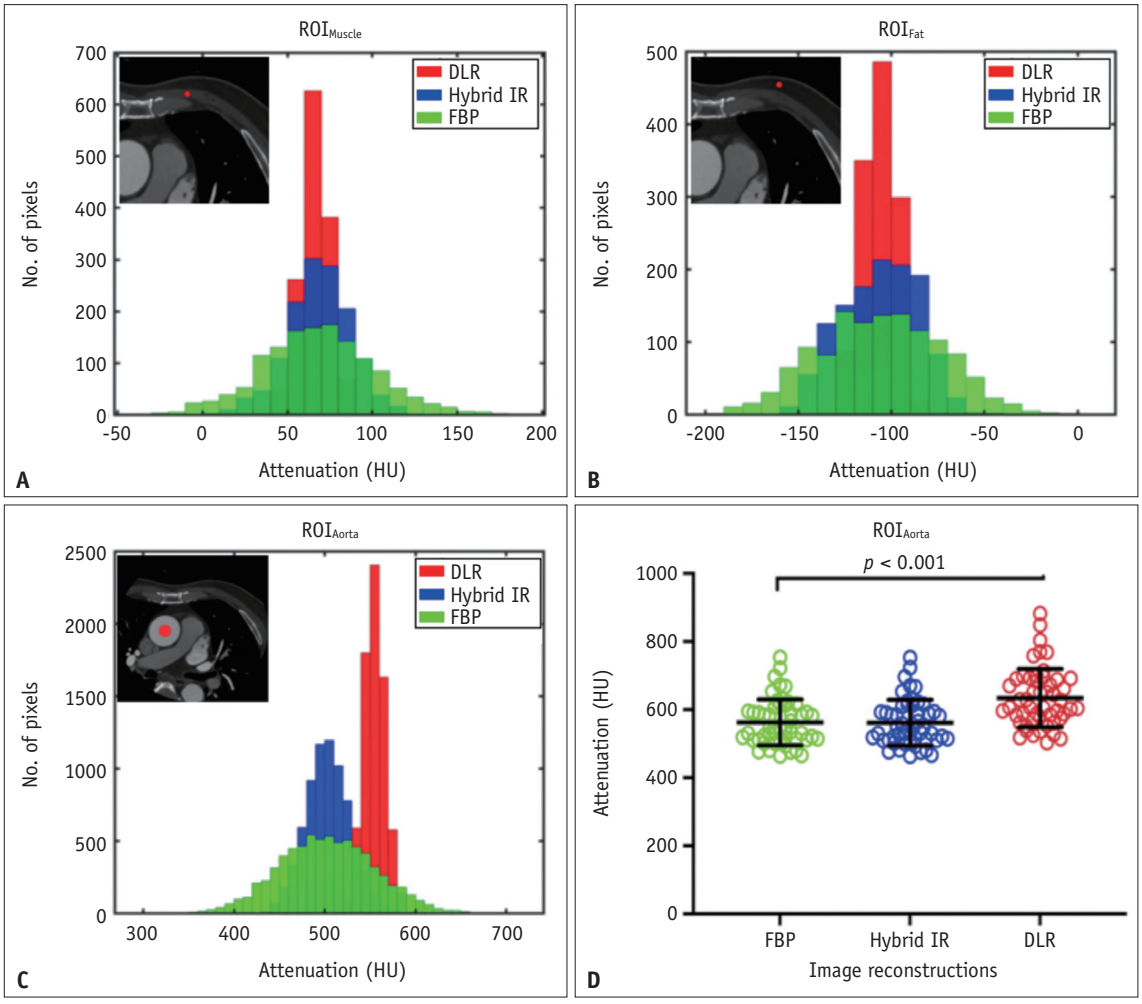

Fig. 3. The histogram analysis of the different image reconstruction methods.
A-D. CT attenuation was measured by placing a circular ROI (red circle) in the muscle **(A)**, fat **(B)**, and aorta **(C)** on the axial CCTA. DLR for red color significantly improves the enhancement of the aorta, while similar attenuation of the muscle and fat is observed. Furthermore, the histograms of DLR have a narrow width that leads to less signal fluctuation and image noise than those of FBP for green color and hybrid IR for blue color. Results of CT attenuation in the aorta among the different image reconstruction methods in fifity-one patients **(D)**. CT attenuation in the aorta was significantly higher with DLR than with FBP or hybrid IR. For a better representation, the comparison of the mean value and standard deviation of the CT attenuation for each type of image reconstruction is illustrated with a solid black line in each result. CCTA = coronary computed tomography angiography, DLR = deep learning reconstruction, FBP = filtered back projection, HU = Hounsfield unit, IR = iterative reconstruction, ROI = region of interest

https://doi.org/10.3348/kjr.2022.0127

Korean Journal of Radiology
KJR

0.001). The CT attenuation of the main coronary arteries was significantly higher in DLR (607.6 ± 90.3) than in the other two image reconstructions (FBP, 332.3 ± 67.9; hybrid IR, 420.3 ± 82.2, $p < 0.001$). Post-hoc Tukey's test revealed significant differences in the main coronary arteries ($p < 0.001$) between any pair of reconstruction methods (FBP vs. hybrid IR, hybrid IR vs. DLR, FBP vs. DLR). In contrast, there was no significant difference in the CT attenuation of fat ($p = 0.586$) and muscle ($p = 0.935$) between the different image reconstruction methods. Post-hoc Tukey's test showed no significant difference in fat (FBP vs. hybrid IR, $p = 0.645$; hybrid IR vs. DLR, $p > 0.999$; FBP vs. DLR, $p = 0.641$) and muscle (FBP vs. hybrid IR, $p = 0.981$; hybrid IR vs. DLR, $p = 0.982$; FBP vs. DLR, $p = 0.929$) between the reconstruction methods. In all coronary arteries, the average SNR and CNR values were significantly higher in DLR than in FBP and hybrid IR ($p < 0.001$). Post-hoc Tukey's test revealed significant differences ($p < 0.001$) between each of the reconstructions (FBP vs. hybrid IR, hybrid IR vs. DLR, FBP vs. DLR).

The histogram plots of the muscle, fat, and aorta at the same level with various image reconstruction algorithms and the range of CT attenuation in the aorta according to the image reconstruction algorithms are shown in Figure 3. The mean HU of the aorta was significantly higher in DLR (633.8 ± 85.6) than that in FBP (562.3 ± 67.5) and hybrid IR (561.2 ± 67.4) ($p < 0.001$). There was a statistically significant difference in CT attenuation of the aorta between FBP and DLR ($p < 0.001$) and hybrid IR vs. DLR ($p < 0.001$), except for FBP vs. hybrid IR ($p = 0.997$). DLR provided a similar HU in fat and muscle compared with FBP and hybrid IR. Furthermore, the histograms of DLR had a narrow width that resulted in less signal fluctuation and image noise than those in FBP and hybrid IR. For a better representation, Figure 3D shows the CT attenuation in the aorta among the different image reconstruction methods in all patients. DLR also showed an overall higher CT attenuation in the aorta compared to FBP and hybrid IR.

Coronary Artery Stent Assessment

The use of DLR resulted in sharper images than those of hybrid IR and FBP when considering the analysis of ERD and ERS. The mean value of ERD was measured as 0.8 ± 0.1 mm for DLR, 1.1 ± 0.2 mm for hybrid IR, and 1.1 ± 0.2 mm for FBP ($p < 0.001$). Post-hoc Tukey's test revealed significant differences ($p < 0.001$) between each of the reconstructions (FBP vs. hybrid IR, hybrid IR vs. DLR, FBP vs. DLR). The mean value of ERS was significantly higher with 1260.4 ± 242.5 HU/mm for DLR when compared with 641.9 ± 112.0 HU/mm for hybrid IR and 801.9 ± 170.7 HU/mm for FBP

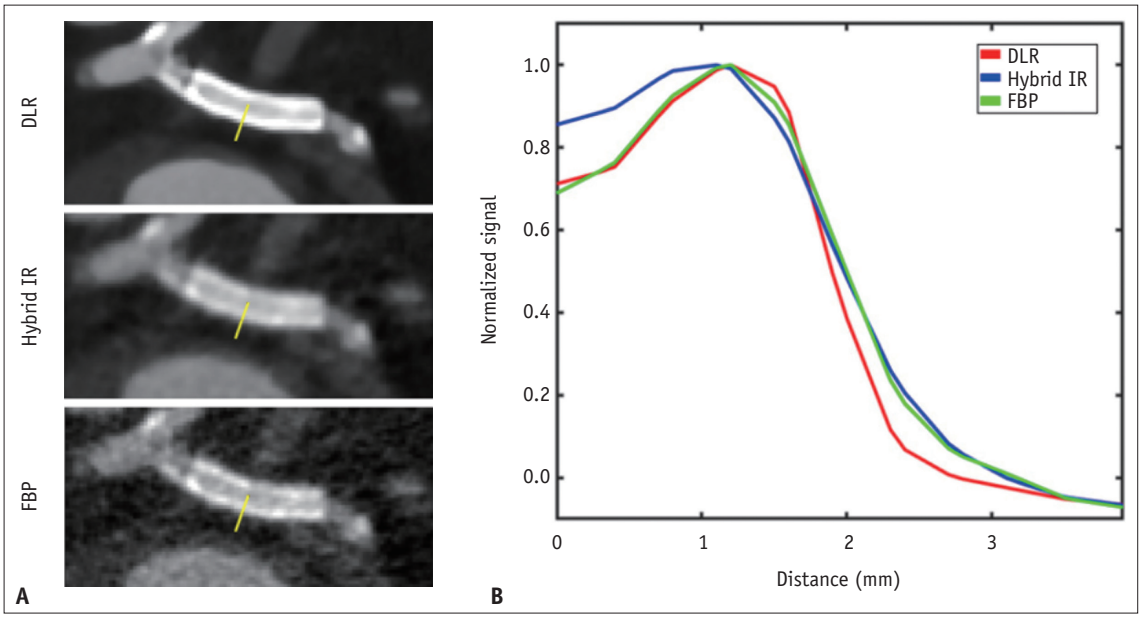

Fig. 4. The example of coronary CT images (A) of the left circumflex artery of a 69-year-old male with coronary stenting obtained using DLR, hybrid IR, and FBP.

A, B. The normalized image profiles are plotted among the various reconstruction methods with a yellow line in panel **(A)**. As demonstrated in panel **(B)**, the higher CT attenuation profile of the coronary stent resulted in a sharper shape that contributed to higher image sharpness on DLR (red line) when compared with that of hybrid IR (blue line) and FBP (green line). DLR = deep learning reconstruction, FBP = filtered back projection, IR = iterative reconstruction

https://doi.org/10.3348/kjr.2022.0127

(p < 0.001). Post-hoc Tukey's test revealed significant differences (p < 0.001) between each of the reconstruction methods (FBP vs. hybrid IR, hybrid IR vs. DLR, FBP vs. DLR). Therefore, these results demonstrate high stent sharpness and low blurring in DLR compared to that of the other. Owing to the reduced blooming artifacts, DLR provided a significantly sharper image profile than FBP and hybrid IR, as shown in Figure 4. There was no significant difference in stent diameter among the three image reconstruction methods (p = 0.646). Post-hoc analysis revealed no significant differences between the reconstructions (FBP vs. hybrid IR, p = 0.990; hybrid IR vs. DLR, p = 0.743; FBP vs. DLR, p = 0.661).

Figure 5 shows that FBP-hybrid IR had better agreement than FBP-DLR and hybrid IR-DLR. The mean difference in stent diameter between FBP and hybrid IR was 0.01 mm (95% confidence interval [CI], -0.32 to 0.35), and the ICC was 0.956 (95% CI, 0.942 to 0.975, p < 0.01). The mean difference in stent diameter between hybrid IR and DLR was 0.06 mm (95% CI, -0.32 to 0.45), and the ICC was 0.944 (95% CI, 0.903 to 0.968, p < 0.01). Similarly, the mean difference in stent diameter between FBP and DLR was 0.08 mm (95% CI, -0.41 to 0.56), and the ICC was 0.928 (95% CI, 0.876–0.959, p < 0.01).

Subjective Image Analysis

The overall image quality, image noise, stent, vessel appearance, and valve apparatus of both observers are summarized in Table 3. The average overall image quality score was significantly greater for DLR (4.1 ± 0.3) than for FBP (2.5 ± 0.3) and hybrid IR (3.1 ± 0.2) (p < 0.001). The image noise was scored superiorly in DLR (4.1 ± 0.5) when compared with hybrid IR (3.0 ± 0.2) and FBP (2.1 ± 0.2) (p < 0.001). Similarly, the vessel appearance score was significantly higher for DLR than for FBP and hybrid IR (Figs. 6, 7). The aortic and tricuspid valve apparatus, including the leaflet, papillary muscle, and chordae tendineae, were more clearly visualized for DLR than for FBP and hybrid IR. The vessel and lumen were evaluated as good delineation in DLR (4.1 ± 0.4), while it was poor and moderate visualization in FBP (2.8 ± 0.4) and hybrid IR (3.1 ± 0.3), p < 0.001. However, the scores for stent evaluation were higher in the DLR group, and there were no significant differences (p = 0.118). The inter-observer agreement was substantial (κ = 0.68) for subjective image analysis.

DISCUSSION

This study investigated quantitative and qualitative measurements of image quality, coronary artery stenting,

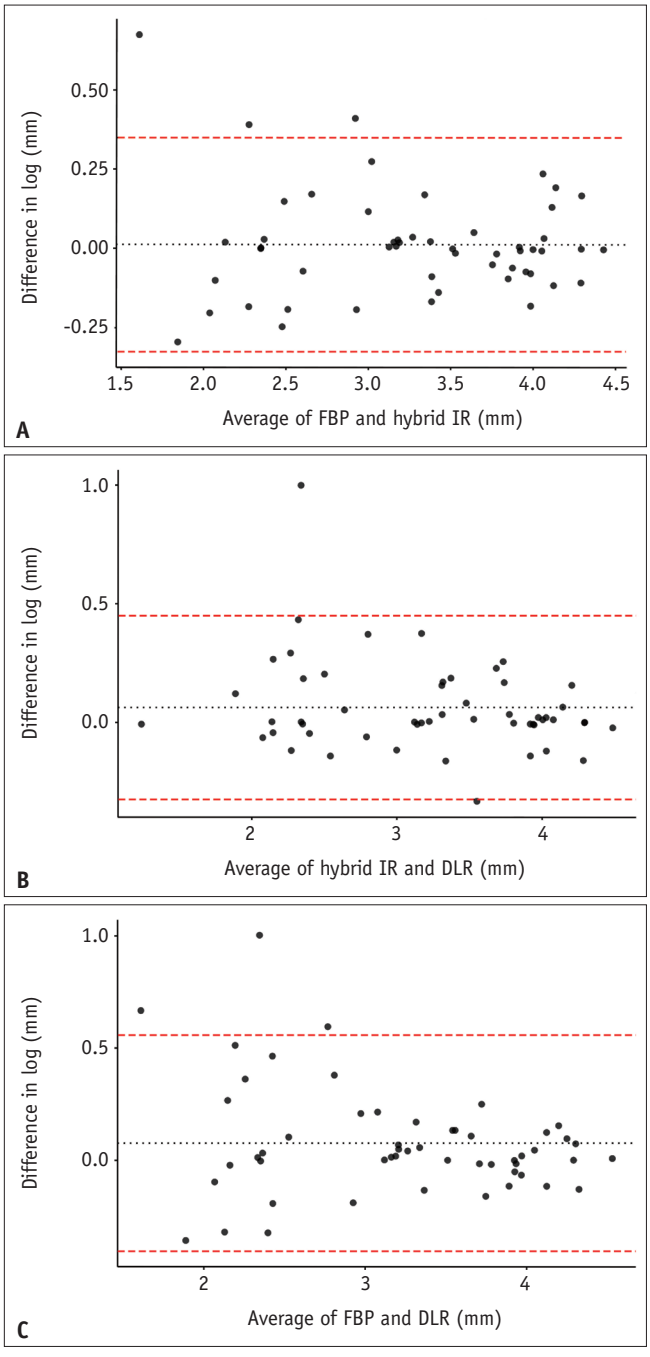

Fig. 5. Bland-Altman analysis on the diameter of the coronary stent by different image reconstructions.
A-C. Bland-Altman plots illustrate diameter of the coronary stent between FBP and hybrid IR **(A)**, hybrid IR and DLR **(B)**, and FBP and DLR **(C)**. The dashed black line represents the mean paired differencen and 95% limits of agreement with dashed red line. DLR = deep learning reconstruction, FBP = filtered back projection, IR = iterative reconstruction

https://doi.org/10.3348/kjr.2022.0127

Korean Journal of Radiology
KJR

Table 3. The Subjective Image Analysis in Three Different Image Reconstructions

	Overall Image Quality	Image Noise	Stent Appearance	Vessel and Lumen	Valve and Chordae Tendinea
FBP	2.5 ± 0.3	2.1 ± 0.2	3.0 ± 0.5	2.8 ± 0.4	3.3 ± 0.4
Hybrid IR	3.1 ± 0.2	3.0 ± 0.2	2.9 ± 0.7	3.1 ± 0.3	3.4 ± 0.5
DLR	4.1 ± 0.3	4.1 ± 0.5	3.4 ± 0.7	4.1 ± 0.4	4.0 ± 0.3
p value	0.001	0.001	0.118	0.001	0.001

Data are the mean ± standard deviation. DLR = deep learning reconstruction, FBP = filtered-back projection, IR = iterative reconstruction

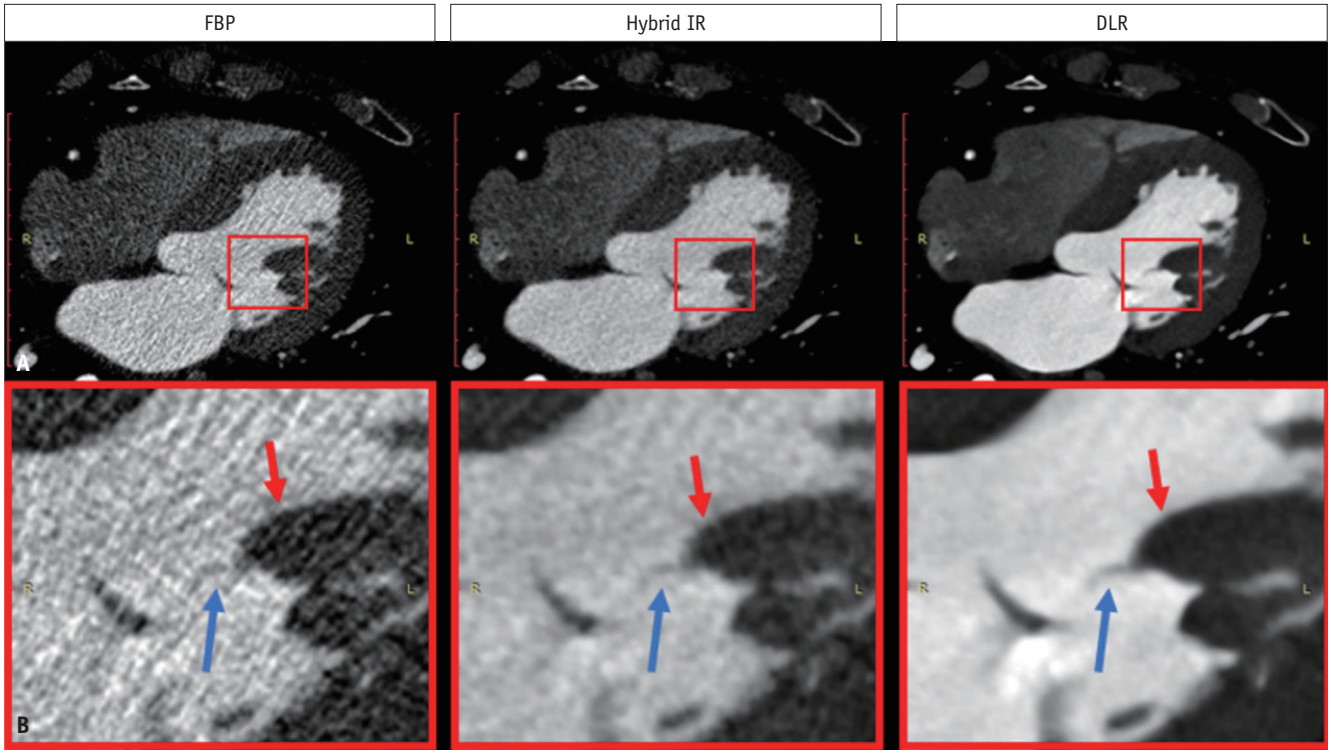

Fig. 6. The visualization of the chordae tendineae and papillary muscle in DLR.
A, B. Chordae tendineae (blue arrows) and papillary muscle (red arrows) are well visualized in DLR images when compared with hybrid IR and FBP **(A)**. The magnified images are among the various reconstruction methods in the red solid box in panel **(B)**. The margin of chordae tendineae and papillary muscles are blurred in FBP and hybrid IR without good differentiation from the surrounding structures when compared with that of DLR. DLR = deep learning reconstruction, FBP = filtered back projection, IR = iterative reconstruction

and visibility of the valve apparatus on CCTA among FBP, hybrid IR, and DLR. In addition, a significant improvement in the SNR and CNR was observed, with a marked decrease in image noise and blooming artifacts with the DLR. The results indicated that the use of DLR for coronary artery stents resulted in superior image quality compared to hybrid IR and FBP. Similarly, subjectively high image quality scores showed an advantageous trend toward DLR. In addition, DLR clearly increased vascular attenuation while maintaining a similar attenuation of the muscles and fat when compared with that of FBP and hybrid IR.

Tatsugami et al. [9] compared the image quality of CCTA between DLR and hybrid IR. In their study, the mean image noise was significantly lower ($p < 0.01$) in DLR than that in hybrid IR. However, they did not quantitatively measure the stents. This study aligns with previous findings that DLR improves image quality with lower image noise and higher SNR and CNR. Furthermore, the results of this study provide additional information that the narrow histogram width of DLR demonstrates less signal fluctuation and image noise than those of FBP and hybrid IR. The histogram shift on the aorta in the DLR can be explained with a high-quality MBIR dataset that selectively boosts CT attenuation in the vessels more than in fat and muscle [8]. In addition, ERD was shorter, and ERS was steeper in the coronary artery stent with DLR when compared with that of hybrid IR and FBP, which could indicate that the blurring of the stent was the lowest in DLR with higher sharpness and lower blooming

 https://doi.org/10.3348/kjr.2022.0127

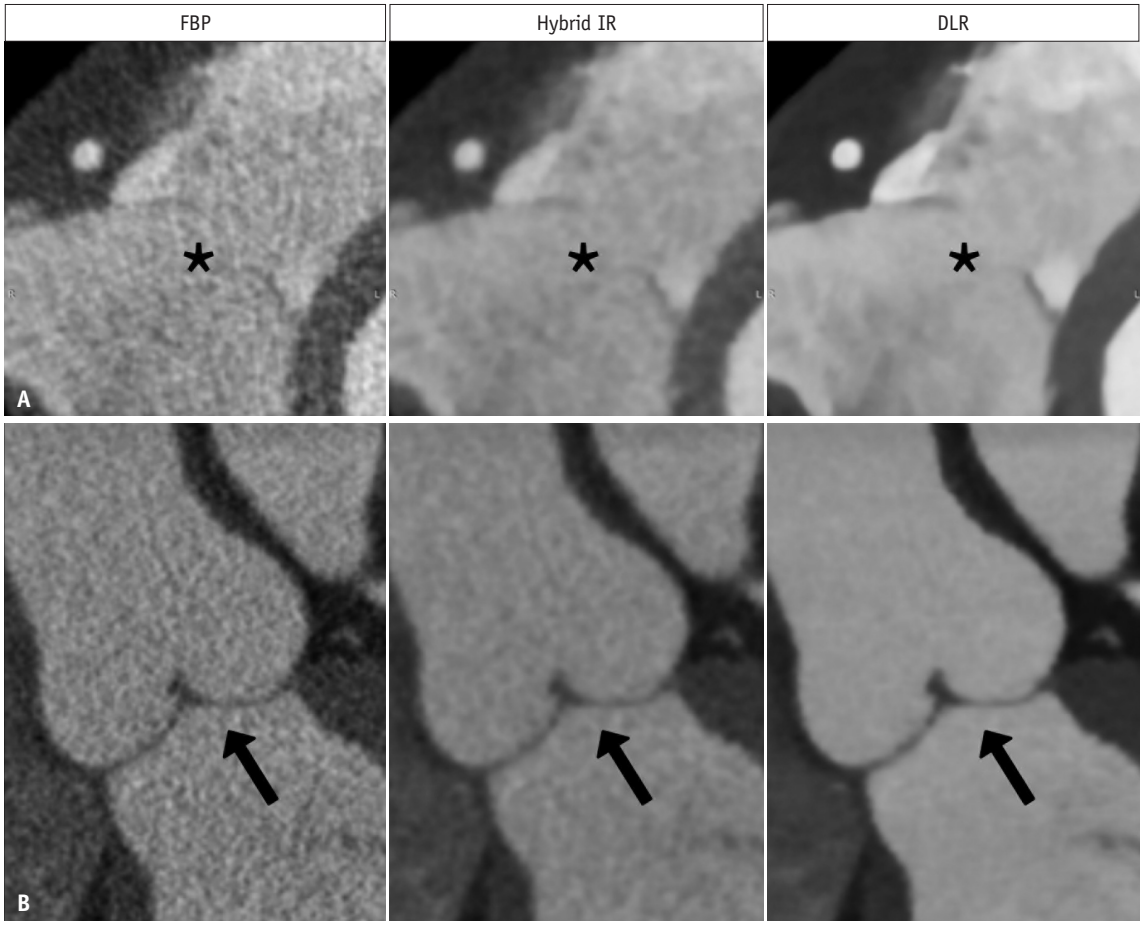

Fig. 7. The depiction of the aortic valve and the tricuspid valve in FBP, hybrid IR, and DLR.
A, B. The clear visualization of the tricuspid valve (**A,** ∗) and aortic valve (**B,** arrows) with lower image noise was observed in the DLR than other image reconstructions. DLR = deep learning reconstruction, FBP = filtered back projection, IR = iterative reconstruction

artifacts. Accurate visualization of the stent allows for the improvement of the diagnostic accuracy of in-stent patency. In this study, we used the medium-sharp kernel of FC14 for hybrid IR, which is the vendor-recommended kernel setting for coronary artery stents. Thus, it could be inferred that hybrid IR demonstrated lower image noise and higher SNR and CNR than FBP, as expected. However, no effect on the stent sharpness was observed. In addition, there was no significant difference in the stent diameter among the three different image reconstructions. The Bland-Altman limits of agreements were -0.32 to 0.35 for FBP and hybrid IR, while it was -0.32 to 0.45 for hybrid IR and DLR. Similarly, the Bland-Altman limits of agreement was -0.41 to 0.56 for FBP and DLR. Conclusively, the agreement in the measurements of stent diameter between FBP and hybrid IR, hybrid IR and DLR, and FBP and DLR was nearly perfect. Further studies considering the application of different options for DLR in the evaluation of blooming artifacts in stents should be conducted. We believe that these results, with higher CNR and SNR in DLR, could allow lower radiation dose scanning with higher image quality.

Moreover, DLR has several potential advantages over other image reconstruction methods. The attenuation of the fat and muscle remained unchanged, while the intravascular attenuation clearly increased with DLR when compared with that of hybrid IR and FBP. A previous investigation [14] achieved higher arterial enhancement with different iodine concentrations of the contrast media to obtain a high-quality diagnostic image without heat discomfort and a lower risk of contrast-enhanced nephropathy. Because higher attenuation of the coronary vessel is desirable for arterial cardiothoracic CTA [15], the use of DLR enables diagnostically satisfactory images without high iodine concentration agents or high delivery rates. In other words, DLR can achieve higher arterial enhancement without using agents with higher iodine concentrations. The selectively increasing vascular enhancement through DLR seems to depend on its training of high-quality images with a high

https://doi.org/10.3348/kjr.2022.0127

Korean Journal of Radiology
KJR

tube current and MBIR, which considers modelling of the system physics, optics, cone beam, scanner statistical noise, and human anatomy, and uses a higher number of iterations in a clinical setting owing to time constraints. Higher CT attenuations in the cystic arteries were reported in model-based iterative reconstruction compared with FBP and hybrid IR [10]. Although there are some advantages to improving vascular enhancement with DLR, an undesired high attenuation artifact may be observed. We speculate that obtaining higher CT attenuation with DLR could be more effective when using a lower iodine concentration of the contrast media.

The use of DLR resulted in an improvement in the visualization of the details of the aortic and tricuspid valve apparatus, including papillary muscle and chordae structure, compared with FBP and hybrid IR (Figs. 6, 7). Furthermore, clear visualization of the valve with DLR allows reliable measurements for preoperative planning of TAVR, TMVR, and TTVR. In general, evaluation of the papillary muscle and chordae tendineae cannot be clearly seen on conventional CT because of its limited spatial resolution. Since lengthening of the chordae tendineae is one of the main findings of mitral regurgitation [16], it is crucial to evaluate the papillary muscle and chordae tendineae. The improved visualization of the chordae structure and papillary muscle in DLR results from its high spatial resolution training with MBIR images. We hypothesize that CCTA with DLR is a promising method for the detection of abnormal phenomena in the papillary muscle and chordae tendineae [8]. The observers also markedly emphasized the clear delineation of the vessel and lumen of the DLR for the visualization of the vessels and lumen. However, the results of ERS and ERD demonstrated a lower reduction of blooming artifacts in DLR, and subjective analysis was equivocal for stent evaluation among different image reconstructions.

However, this study had some limitations. the study population was relatively small. Moreover, we did not evaluate blooming artifacts in the stent by categorizing its materials or diameter. This study investigated the effects of DLR on CCTA in terms of the overall image quality. Therefore, further studies are required by enrolling more patients with coronary artery stents to confirm the results of this study. Moreover, we investigated the effects of various reconstruction algorithms on Aquilion ONE Prism. The effects of other DLR algorithms and CT vendors may differ. In addition, the body-sharp option was selected for deep learning image reconstruction. Therefore, different options and strengths of DLR should be conducted for stent evaluation in the near future. Further studies are required to evaluate whether the improvement in image quality by the DLR method contributes to the accurate interpretation of abnormal changes, even with low-osmolality contrast media for CCTA. Finally, the combination of a high concentration of iodinated contrast media and DLR could produce undesired artifacts. On the other hand, this would be effective when using both DLR and a lower concentration of contrast media, which decreases the heat discomfort for patients following administration of a high concentration of contrast media. The effect of DLR on the iodine concentration of the contrast media needs to be investigated.

In conclusion, DLR reconstruction provided better results than hybrid IR and FBP reconstruction in terms of image quality and blooming artifacts in CCTA. DLR yielded better visualization of the valve apparatus and higher contrast enhancement.

Availability of Data and Material

The datasets generated or analyzed during the study are available from the corresponding author on reasonable request.

Conflicts of Interest

The co-authors (J. K. Ryu and H. Shim) are employee Canon Medical Systems Korea, Seoul, Korea that is the subsidiary in Korea of Canon Medical Systems Corporation, Otawara-si, Japan.

Author Contributions

Conceptualization: all authors. Data curation: Chuluunbaatar Otgonbaatar, Jae-Kyun Ryu, Jaemin Shin. Formal analysis: Chuluunbaatar Otgonbaatar, Jae-Kyun Ryu. Funding acquisition: Jae-Kyun Ryu, Hackjoon Shim. Investigation: Chuluunbaatar Otgonbaatar, Jae-Kyun Ryu. Methodology: Ji Young Woo, Jung Wook Seo, Dae Hyun Hwang. Project administration: Hackjoon Shim, Dae Hyun Hwang. Resources: Chuluunbaatar Otgonbaatar, Jae-Kyun Ryu, Jaemin Shin. Software: Chuluunbaatar Otgonbaatar, Jae-Kyun Ryu. Supervision: Hackjoon Shim, Dae Hyun Hwang, Jung Wook Seo, Ji Young Woo. Validation: Chuluunbaatar Otgonbaatar, Jae-Kyun Ryu. Visualization: Chuluunbaatar Otgonbaatar, Jae-Kyun Ryu. Writing—original draft: Chuluunbaatar Otgonbaatar, Jae-Kyun Ryu. Writing—review & editing: Hackjoon Shim.

 https://doi.org/10.3348/kjr.2022.0127

ORCID iDs
Chuluunbaatar Otgonbaatar
https://orcid.org/0000-0002-8533-6165
Jae-Kyun Ryu
https://orcid.org/0000-0003-1926-042X
Jaemin Shin
https://orcid.org/0000-0001-6205-8222
Ji Young Woo
https://orcid.org/0000-0002-6200-0159
Jung Wook Seo
https://orcid.org/0000-0002-5975-8698
Hackjoon Shim
https://orcid.org/0000-0002-6731-0084
Dae Hyun Hwang
https://orcid.org/0000-0003-1995-6312

Funding Statement
None

REFERENCES

1. Halliburton SS, Tanabe Y, Partovi S, Rajiah P. The role of advanced reconstruction algorithms in cardiac CT. *Cardiovasc Diagn Ther* 2017;7:527-538
2. Blanke P, Naoum C, Webb J, Dvir D, Hahn RT, Grayburn P, et al. Multimodality imaging in the context of transcatheter mitral valve replacement: establishing consensus among modalities and disciplines. *JACC Cardiovasc Imaging* 2015;8:1191-1208
3. Naoum C, Blanke P, Cavalcante JL, Leipsic J. Cardiac computed tomography and magnetic resonance imaging in the evaluation of mitral and tricuspid valve disease: implications for transcatheter interventions. *Circ Cardiovasc Imaging* 2017;10:e005331
4. Willson AB, Webb JG, Labounty TM, Achenbach S, Moss R, Wheeler M, et al. 3-dimensional aortic annular assessment by multidetector computed tomography predicts moderate or severe paravalvular regurgitation after transcatheter aortic valve replacement: a multicenter retrospective analysis. *J Am Coll Cardiol* 2012;59:1287-1294
5. Choe J, Koo HJ, Kang JW, Kim JB, Kang HJ, Yang DH. Aortic annulus sizing in bicuspid and tricuspid aortic valves using CT in patients with surgical aortic valve replacement. *Sci Rep* 2021;11:21005
6. Lenfant M, Chevallier O, Comby PO, Secco G, Haioun K, Ricolfi F, et al. Deep learning versus iterative reconstruction for CT pulmonary angiography in the emergency setting: improved image quality and reduced radiation dose. *Diagnostics (Basel)* 2020;10:558
7. Akagi M, Nakamura Y, Higaki T, Narita K, Honda Y, Zhou J, et al. Deep learning reconstruction improves image quality of abdominal ultra-high-resolution CT. *Eur Radiol* 2019;29:6163-6171
8. Higaki T, Nakamura Y, Zhou J, Yu Z, Nemoto T, Tatsugami F, et al. Deep learning reconstruction at CT: phantom study of the image characteristics. *Acad Radiol* 2020;27:82-87
9. Tatsugami F, Higaki T, Nakamura Y, Yu Z, Zhou J, Lu Y, et al. Deep learning-based image restoration algorithm for coronary CT angiography. *Eur Radiol* 2019;29:5322-5329
10. Hamamura T, Hayashida Y, Takeshita Y, Sugimoto K, Ueda I, Futatsuya K, et al. The usefulness of full-iterative reconstruction algorithm for the visualization of cystic artery on CT angiography. *Jpn J Radiol* 2019;37:526-533
11. Tatsugami F, Higaki T, Sakane H, Fukumoto W, Kaichi Y, Iida M, et al. Coronary artery stent evaluation with model-based iterative reconstruction at coronary CT angiography. *Acad Radiol* 2017;24:975-981
12. Karlo C, Leschka S, Goetti RP, Feuchtner G, Desbiolles L, Stolzmann P, et al. High-pitch dual-source CT angiography of the aortic valve-aortic root complex without ECG-synchronization. *Eur Radiol* 2011;21:205-212
13. Yan C, Zhou G, Yang X, Lu X, Zeng M, Ji M. Image quality of automatic coronary CT angiography reconstruction for patients with HR ≥ 75 bpm using an AI-assisted 16-cm z-coverage CT scanner. *BMC Med Imaging* 2021;21:24
14. Weininger M, Barraza JM, Kemper CA, Kalafut JF, Costello P, Schoepf UJ. Cardiothoracic CT angiography: current contrast medium delivery strategies. *AJR Am J Roentgenol* 2011;196:W260-W272
15. Fleischmann D. Use of high concentration contrast media: principles and rationale-vascular district. *Eur J Radiol* 2003;45 Suppl 1:S88-S93
16. Ryan R, Abbara S, Colen RR, Arnous S, Quinn M, Cury RC, et al. Cardiac valve disease: spectrum of findings on cardiac 64-MDCT. *AJR Am J Roentgenol* 2008;190:W294-W303